The Advection–Diffusion Problem for Stratospheric Flow. Part I: Concentration Probability Distribution Function

Y. HU AND R. T. PIERREHUMBERT

Department of the Geophysical Sciences, The University of Chicago, Chicago, Illinois

(Manuscript received 13 March 2000, in final form 8 November 2000)

ABSTRACT

The mixing of a passive tracer by realistic time-dependent stratospheric flow (European Centre for Medium-Range Weather Forecasts winds) on an isentropic surface (420 K) is studied. Simulations of the advection–diffusion problem for an initially large-scale tracer field are carried out in the limit of weak diffusivity. Owing to chaotic advection, tracer variance is cascaded to small scales, where it can be dissipated despite the weak diffusivity. The tracer fluctuations are characterized in terms of their probability distribution function (PDF). The PDFs are characterized by a Gaussian core and ''fat tails,'' which fall more slowly than a Gaussian, and indicate anomalously high probability of extreme concentration fluctuations. Given the nonlinearity of many chemical reactions of interest, the anomalous prevalence of extreme fluctuations could have a profound effect on reactive tracers.

Zonal variations of tracer are homogenized globally leading to a unimodal PDF. Initially meridional variations are strongly influenced by the presence of mixing barriers. Meridional gradients homogenize only within mixing zones of limited latitudinal extent, bounded by permeable mixing barriers. The PDF becomes multimodal, with distinct populations of air caused by blending of the concentration values within each mixing zone. The Tropics is a zone of weak mixing, and serves as an important repository of stratospheric tracers, which are episodically ejected into surf zones in the form of filaments bearing extreme concentration values.

The shapes of the PDFs are discussed in terms of theoretical methods developed in the context of highly idealized mixing models. It is shown that such methods retain their utility when applied to realistic stratospheric mixing. The role of the probability distribution of finite-time Lyapunov exponents for the underlying trajectory problem is highlighted. The use of conditional averages of diffusion and dissipation is also illustrated. PDFs yielded by the idealized advection–diffusion problem are found to resemble those appearing in a GCM simulation of N_2O.

The theoretical arguments and numerical results imply that under the assumption that the diffusivity is set so that the dissipation scale is comparable to model resolution, the concentration PDF eventually reaches a universal shape independent of model resolution after an initial transient stage. However, the width of the distribution, or equivalently the variance of the tracer fluctuation, increases algebraically as model resolution is refined.

1. Introduction

Many problems of interest in the atmospheric sciences critically involve mixing, and one of the central problems in mixing is the characterization of the fluctuations of tracer concentrations. The past decade has seen a renaissance of interest in the behavior of probability distribution functions (PDFs) of advected scalar tracers such as chemical concentration, temperature, or two-dimensional vorticity. The tracer PDF, equivalent to the histogram of tracer values, measures the chance of finding a given tracer concentration value taken over a spatial domain, over time at a single point, or (less commonly in practice) over an ensemble of realizations of the mixing process.[1] In addition to the PDF of the tracer itself, one can also study the PDF of tracer gradients, or of tracer differences over finite time or space intervals. Tracer PDFs have been used extensively to study mixing in laboratory experiments (Castaing et al. 1989; Jayesh and Warhaft 1991; Gollub et al. 1991), and the theory of the shape of the PDFs of advected–diffused passive tracers has become quite well developed for a range of highly idealized situations (Sinai and Yakhot 1989; Pumir et al. 1991; Majda 1993; Shraiman and Siggia 1994; Chertkov et al. 1995; Balkovsky and Fouxon 1999). A survey of some of the key developments

Corresponding author address: Dr. Yongyun Hu, Dept. of Applied Mathematics, University of Washington, P.O. Box 352420, Seattle, WA 98195-2420.
E-mail: yongyun@amath.washington.edu

[1] In some literature, PDF is the abbreviation for probability density function. The relation between the probability distribution function and probability density function is $P(a < \theta < b) = N \int_a^b p(\theta)\, d\theta$, where N is the total sample, and $p(\theta)$ is the probability density function. More precise definitions of both can be found in many text books on statistics or statistical fluid mechanics, for example, Lumley (1970).

in both experiments and theories can be found in Pierrehumbert (2000), Sreenivasan and Antonia (1997), and Warhaft (2000). A comprehensive review by Majda and Kramer (1999) covers additional aspects of the theoretical progress of the PDFs, particularly covering cases of advection by random unidirectional shear, and action of small-scale velocity fields on large-scale tracer fluctuations (the ''homogenization problem'').

The new outlook on PDFs has the potential of being useful in many problems of pressing atmospheric interest. Stratospheric chemistry problems promise to be particularly fruitful area of application. Many chemical reactions of interest have reaction rates that are nonlinear functions of the concentrations, with the result that bulk reaction rates are sensitive to tracer fluctuations and not just mean tracer values. A specific example of how this might play out can be found in Edouard et al. (1996), who found that ozone destruction rates can be sensitive to resolution of small scales in the tracer field. One would like to know, from a theoretical standpoint, how ozone destruction in such problems scales with resolution, and whether the resolution beyond which the destruction rate converges is practically achievable. An appreciation of the importance of mixing in determining ozone destruction can be obtained from Tan et al. (1998). Apart from applications to chemistry, study of the tracer PDF may provide a means to assess the aggregate importance of small-scale episodic dissipative events, such as those due to gravity wave breaking, that are difficult to observe directly. Some aspects of the use of tracer patterns in the diagnosis of dissipation were discussed in Haynes and Anglade (1997). Ultimately, the use of PDF methods may provide a means to systematize and extend this approach.

Existing theory for the PDFs of an advected tracer subject to small-scale diffusion has made significant strides, but still rests on idealizations that prevent direct application to realistic atmospheric flows. Such complications include the existence of transport barriers, of anisotropy, and of the nature of sources and sinks of realistic chemical constituents. The aim of the present work is to carry out simulations of the problem of advection–diffusion by realistic stratospheric winds on an isentropic surface, and to see to what extent the behavior of the PDF can be understood in terms of concepts arising from more idealized theories. The stratospheric case provides an ideal forum for such inquiries, as the advecting flow field is very spatially smooth, and the flow can be regarded as nearly two-dimensional over the timescales of interest in the present work. As a first step, in the following we restrict attention to a passive tracer, investigate only the PDF of the tracer field itself, and explore only the initial-value problem. Subsequent papers will take up the PDF of tracer gradients, tracer differences over finite separation distances, and the equilibrium source/sink case.

There has already been a great deal of work on the pure advection problem in the stratosphere (e.g., Pierrehumbert 1991; Waugh and Plumb 1994; Waugh et al. 1997) and troposphere (e.g., Pierrehumbert 1991, 1998; Pierrehumbert and Yang 1993). This work has focused on the implications of exponentially rapid generation of small scale filaments, and of the fact that large-scale winds can be used to reconstruct aspects of the tracer field at scales far smaller than resolved in the wind field. The work of Waugh and Plumb (1994) was particularly important in demonstrating the occurrence of the predicted filaments in the real atmosphere. Without the incorporation of dissipation, it is difficult for this enterprise to proceed further. Because in the absence of diffusion tracer gradients continue to amplify exponentially for all time, which is unrealistic. The choice of time intervals for pure advection is carried out currently without much theoretical guidance [a recent study on this issue can be found in Methven and Hoskins (1999)]. Dissipation, however, introduces an intrinsic memory time into the process. Our goal in the present paper is to go beyond the subject of chaotic advection, to the subject of chaotic advection–diffusion.

The theoretical developments of potential use to us are summarized in section 2. Our simulation method is described in section 3. Following a discussion of the statistics of the Lyapunov exponents in section 4, we describe the fundamental character of the simulated mixing in section 5. A recapitulation of the main points is given in section 6.

2. Theoretical considerations

We shall be concerned with the evolution of a passive tracer with concentration θ, governed by the equation

$$\frac{\partial \theta}{\partial t} + \mathbf{v} \cdot \boldsymbol{\nabla} \theta = \kappa \nabla^2 \theta, \tag{1}$$

subject to the following restrictions: 1) The advecting flow is two-dimensional and nondivergent. 2) The equation is solved on a spatially bounded domain, which is taken to be a spherical surface in the calculations below. 3) The velocity field is spatially smooth, in the sense that $|\boldsymbol{\nabla}\mathbf{v}|$ is finite everywhere. The velocity fields of principal concern are time-dependent with a nonzero correlation time, but are not generally temporally periodic. 4) We study the advection–diffusion problem in the limit of large Peclet number, $\mathrm{Pe} = VL/\kappa \gg 1$, where V and L are the characteristic scales of velocity and eddy length, respectively, and κ is diffusivity.

In the present work, we confine our attention to the transient evolution of an initial concentration field as it proceeds toward a well-mixed state. The properties of (1) can be understood in terms of the properties of the trajectory problem for the velocity $\mathbf{v}$, that is, $d\mathbf{r}/dt = \mathbf{v}$. The quantity of key interest is the rate of separation of neighboring trajectories. For the flows we shall consider, nearby trajectories separate exponentially in time, for either the forward or backward trajectory problem. This property is generic to most time-dependent spa-

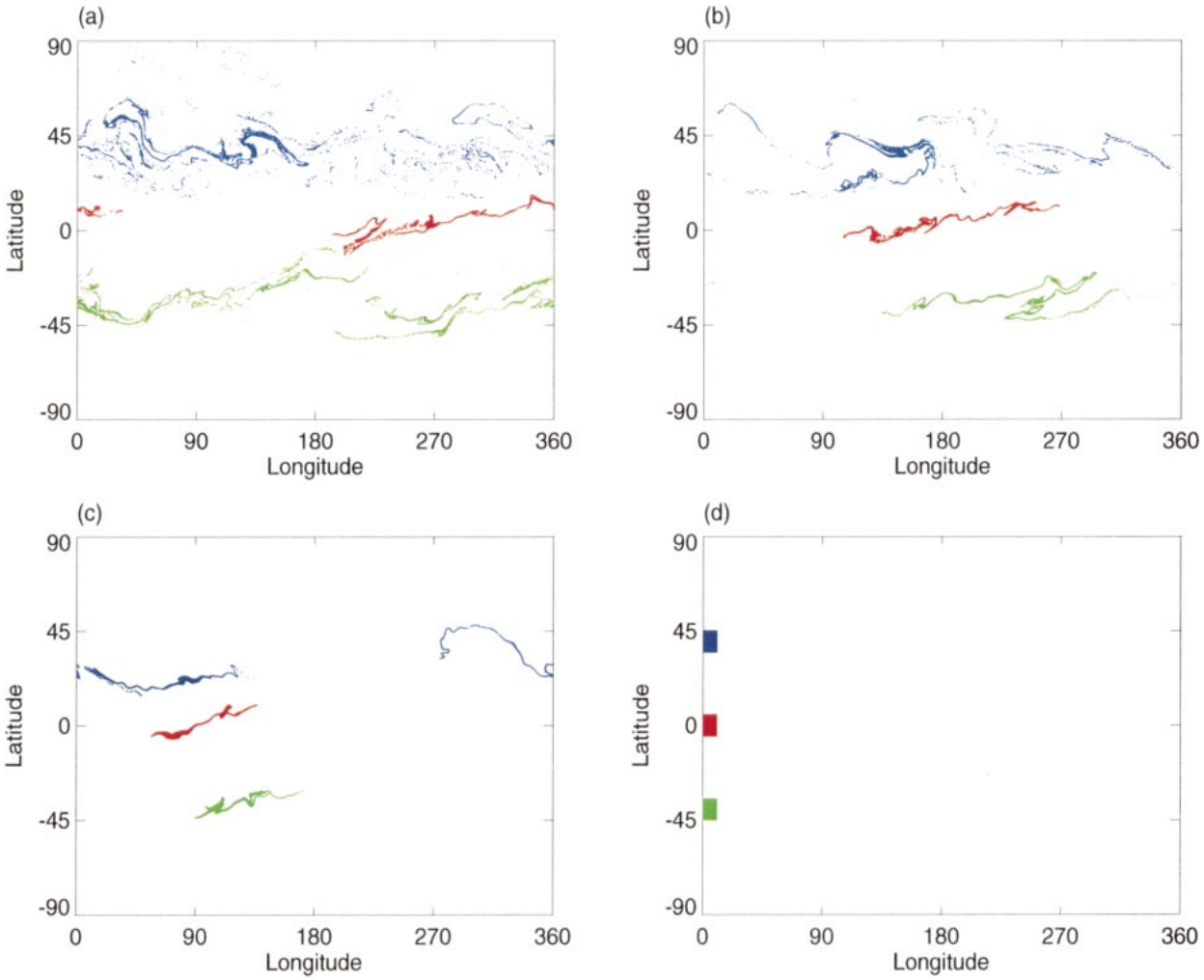

FIG. 1. Backward-trajectory calculation from 30 Aug to 1 Jul. Three blobs of particles are initially released in three 10° × 10° areas on 30 Aug. Each particle blob consists of 100 × 100 particles. (a) Day −60 (1 Jul), (b) day −40, (c) day −20, (d) day 0.

tially smooth flows, particularly flows that are aperiodic in time. The exponential rate of separation, evaluated over a finite stretch of time T, is known as the finite-time Lyapunov exponent (FTLE). The use of FTLEs in characterizing mixing in atmospheric flows was discussed in Pierrehumbert (1991) and Pierrehumbert and Yang (1993). A review of the role of the FTLEs in the advection–diffusion problem can be found in Pierrehumbert (2000). The FTLE varies from trajectory to trajectory, so the separation rate for the whole flow is not characterized by a single number, but rather by the histogram (PDF) of the FTLEs over an ensemble of trajectories.

The FTLEs for the back-trajectory problem enter the problem for the PDF of θ as follows. Suppose we want to know the value of θ at a given point $\mathbf{r}_0$ at time t after the initial condition is imposed. Let the FTLE for the back-trajectory problem emanating from $\mathbf{r}_0$ be λ. Now suppose that diffusion homogenizes the tracer over a length r_d. This dissipation scale is determined by balancing the strain rate against the outward diffusion, yielding

$$r_d = \left(\frac{\kappa}{\lambda}\right)^{1/2}, \tag{2}$$

the so-called Batchelor dissipation scale (Batchelor 1959). Now, to determine the concentration near $\mathbf{r}_0$, we draw a disk of diameter r_d around $\mathbf{r}_0$, and ask where the fluid arriving in this disk *came from* at time $t = 0$. The place the tracer came from is found by running the back trajectory problem for a dense cloud of points filling out the disk. Because of exponential separation of trajectories, the disk maps back to a thin filament of length $r_d \exp(\lambda t)$. The value of $\theta(\mathbf{r}_0)$ is then the average over this long filament of the initial values of θ. An example of a calculation of the source-air for realistic stratospheric flow is shown in Fig. 1. If the characteristic length scale of the initial tracer blob is L, then the average along the filament is the mean of $M = (r_d/L)$

$\exp(\lambda t)$ independent random concentrations, and so by the central limit theorem, the PDF of θ should be Gaussian, with a variance proportional to M^{-1}. This variance goes to zero exponentially, as t becomes large, and the decay rate is λ.

Figure 1 also illustrates a property of backward trajectories that will pervade all our subsequent discussion of mixing by realistic stratospheric flow. Although the filament is indeed exponentially long, the domain it traverses is very anisotropic. It spreads out rapidly over the entire zonal domain, on account of the strong zonal jets. The meridional width of the domain sampled grows much more slowly in time. The implications of this point for undiffused pure advection were discussed in Pierrehumbert and Yang (1993). The net result is that meridional tracer variations are sampled only over a limited range of latitudes, which expands only slowly in time. Viewed from the standpoint of the forward in time mixing problem, meridional variations are mixed only over a limited width mixing region. The mixing region grows slowly in time, if at all.

The preceding argument only implies Gaussianity of the PDF taken over those portions of the domain with a given λ. The tracer field consists of a tangle of intertwined tracer filaments of various thickness and lengths. Tracer filaments arising from large λ are thin in proportion to $\lambda^{-1/2}$, are long in proportion to $\exp(\lambda t)$ and exhibit concentration fluctuations that are small in proportion to $\exp(-\lambda t)$. Neighbors of such filaments will soon become overlapped (mixed) due to diffusion, which yields homogenization. In contrast, filaments arising from small λ are short and thick, and have anomalously large concentration fluctuations against diffusion. It is these filaments that dominate the large θ tails of the PDF taken over the whole domain. Since each part of the tail of $P(\theta)$ arises from a *different* Gaussian distribution, the overall form of $P(\theta)$ can be non-Gaussian.

The rate of collapse of the Lyapunov PDF to a spike is important, because it determines how the improbability of low FTLEs plays out against the fact that parts of the flow with anomalously low FTLEs have exponentially weaker decay of the tracer fluctuations. A quantitative discussion of this point can be found in Pierrehumbert (2000) and Balkovsky and Fouxon (1999). Typically, the large θ tails are flatter than Gaussian, generally either exponential or stretched exponential. A PDF which has tails flatter than Gaussian for large values of its argument is referred to as having ''fat tails.'' Fat tails are important, because they imply an anomalously high probability of extreme events.

From the above picture we can gain some insight as to how the concentration fluctuations depend on κ, which for any given advecting flow is equivalent to varying r_d. Since numerical simulations are generally constructed with an explicit or numerical diffusivity that assures that the dissipation scale is of the same order of magnitude as the grid scale, varying r_d is also equivalent to varying model resolution. For the freely decaying case we pose the question as follows: For a given large-scale initial condition θ_0 with zero mean, how does the concentration standard deviation $\sigma(t)$ at a later time t depend on r_d? It is well established that, after a sufficiently long time has passed, σ decays exponentially at a rate that is independent of r_d and that is proportional (though not equal) to the most probable FTLE (Pierrehumbert 1994, 2000; Antonsen et al. 1996). This exponential decay only sets in after sufficient time has passed for the initial tracer variance to cascade down to the dissipation scale. This time delay is the mix-down time, $t_*(r_d) = (a/\lambda)\ln(L/r_d)$, where L is the initial tracer scale and a is an order unity constant. Dissipation affects the magnitude of tracer fluctuations primarily through its effect on t_*. At large times, the time series can be approximated by

$$\sigma(t, \lambda, r_d) = \sigma_0 e^{-b\lambda[t - t_*(r_d)]}, \tag{3}$$

where b is an order unity constant, and λ in this expression refers to the dominant FTLE. Substituting for t_* we then find that the ratio of tracer fluctuation amplitudes between simulations with resolution $r_d = r_1$ and $r_d = r_2$ is

$$\frac{\sigma(t, \lambda, r_1)}{\sigma(t, \lambda, r_2)} = \left(\frac{r_1}{r_2}\right)^{-ab}. \tag{4}$$

In other words, the tracer fluctuation amplitude increases like a power of the resolution, as resolution is refined. The exponent is an order unity quantity that depends only on the statistics of the advecting flow.

The effect of resolution on the shape of the PDF at a fixed time proceeds from reasoning very similar to that that led to (4). The PDF is a weighted average of Gaussians with standard deviations σ given by (3), weighted according to the probably of the corresponding FTLE λ. Now, Eq. (4) tells us that changing the resolution changes all the σ going into this average by a fixed proportion which is independent of λ. Hence, at times large enough for Eq. (4) to apply, resolution affects the overall width of the PDF, but not its shape. Additionally, because of the effect of resolution on mix-down time, as resolution is increased one has to wait longer and longer for the remote tails of the PDF to converge to their asymptotic form. The farther out on the tails one goes, the longer one has to wait.

Further insight into the tracer PDF can be obtained from the PDF transport equation, which is the evolution equation that the concentration PDF obeys. The derivation of the PDF transport equation is summarized in Pierrehumbert (2000). In the absence of tracer forcing, it is

$$\partial_t P = -\kappa\partial_\theta[P(\theta)\langle\nabla^2\theta\rangle_\theta] \tag{5}$$

$$= -\kappa\partial_{\theta\theta}[P(\theta)\langle|\nabla\theta|^2\rangle_\theta], \tag{6}$$

where $\langle\ldots\rangle_\theta$ represents the conditional average of the

indicated quantity over all parts of the domain where θ takes on the specified value. Equation (6) is a reversed-time diffusion equation. If the conditional dissipation is independent of θ, then the equation admits a particular solution which consists of a Gaussian PDF that collapses onto a spike as time progresses. Non-Gaussian behavior is associated with nonconstant conditional dissipation. If the conditional dissipation increases with $|\theta|$, then the tails of the PDF decay more slowly than a Gaussian. Explicit formulas linking the tracer PDF to the conditional dissipation in the case of exponentially decaying tracer variance can be found in Eswaran and Pope (1988) and Sinai and Yakhot (1989). For the reasons discussed in Pierrehumbert (2000), the conditioned-diffusion form of the PDF transport equation, Eq. (5), imposes no constraint on the shape of the tracer PDF in the decaying case.

Ching and Kraichnan (1998) have derived a general formula linking the PDF to the conditional dissipation and conditional diffusion. They show that

$$P(\theta) = \frac{C}{\langle|\nabla\theta|^2\rangle_\theta} \exp\left(\int_0^\theta \frac{\langle\nabla^2\theta\rangle_X}{\langle|\nabla\theta|^2\rangle_X}\, dX\right), \qquad (7)$$

where C is a normalization constant. Surprisingly, this equation is purely kinematic; it is valid for any differentiable field θ, whether or not the field satisfies Eq. (1). A closely related formula was derived earlier by Nakamura (1996) as a step in the derivation of the modified Lagrangian mean mixing formulation. In the simplest case, if tracer is dissipated in structures characterized by a unique length scale, then simple scaling shows that the conditional diffusion is linear in θ and that the conditional dissipation is independant of θ. In this case Eq. (7) implies that the PDF is Gaussian. If the conditional diffusion remains linear in θ, corresponding to a constant mean decay rate, but fluctuations cause the conditional dissipation to increase with θ, then fat tails result. This is precisely the situation we will encounter in our atmospheric simulations.

In the above, we have established some tools that have emerged from the theoretical literature on advection–diffusion. They are examination of PDFs of concentration, examination of the PDFs of finite-time Lyapunov exponents, and examination of conditional diffusion and dissipation. In subsequent sections we shall bring these tools to bear on an analysis of a realistic stratospheric mixing problem.

3. Data and simulation method

The advection–diffusion equation is solved on the sphere using a high-resolution finite-volume (van Leer) numerical scheme. A full description of the numerical method can be found in van Leer (1977), Peyret and Taylor (1983), and Putti et al. (1990). This numerical method was first applied to atmospheric advection–diffusion reaction by Edouard et al. (1996). The van Leer class of numerical schemes is attractive for tracer problems, since it prevents the formation of spurious negative tracer values in the wake of sharp gradients, while minimizing undesirable numerical smoothing. The simulations are run without explicit diffusion. The numerical scheme has the effect of introducing diffusion just sufficient to damp out variations at the scale of the resolution.

In the present study, the globe is covered by 327 680 equilateral triangles, projected onto the spherical surface from an inscribed icosahedron. The resolution (distance between the centroids of two neighboring triangles) is about 30 km, and a time step of approximately 2.5 min is sufficient to assure numerical stability. The triangular grid has the advantage of covering the entire sphere with nearly uniform resolution, so that numerical effort is not wasted on excessive resolution at the poles. It also removes the singularity at the poles, which most of the atmospheric models with rectangular grids have to deal with.

The winds used for driving tracer advection are derived from the analysis of the European Centre for Medium-Range Weather Forecasts (ECMWF) for the year 1992. Pressure-level winds are first vertically interpolated to the 420 K isentropic surface, which is about 15 km high from the ground and above the tropopause everywhere. The small divergent wind component is removed, and the resulting projection on the nondivergent wind is used to derive the streamfunction on the ($2.5° \times 2.5°$) ECMWF grid. The streamfunctions are then interpolated onto the vertices of each triangle. Tracer concentrations are calculated at the centroids of triangles.

4. Lyapunov exponent PDF

Since the behavior of the FTLE occupies such a central role in the advection–diffusion problem, we first present some typical results for the PDF of the FTLEs for the stratospheric flows under consideration. The values were computed using the eigenvalue method used in Pierrehumbert and Yang (1993), retaining only the largest FTLE. The PDFs are computed over an ensemble of forward trajectories initialized on a 1° latitude–longitude grid, with contribution weighted according to area. Of particular interest is the rate at which the PDF of the FTLEs collapses to a spike as time goes on.

Figure 2 shows the Lyapunov exponent PDFs for trajectories started on 1 August, with the FTLE computed at 10, 20, and 30 August. The first thing to note is that the trajectory problem is indeed chaotic, in the sense that neighboring trajectories separate exponentially, with the exception of very rare trajectories that have zero or near-zero FTLE. There are in fact a very few trajectories (mostly in the Tropics) that have negative FTLEs; this situation arises because the FTLEs were computed using the full analyzed ECMWF wind rather than the projection on the nondivergent component, and

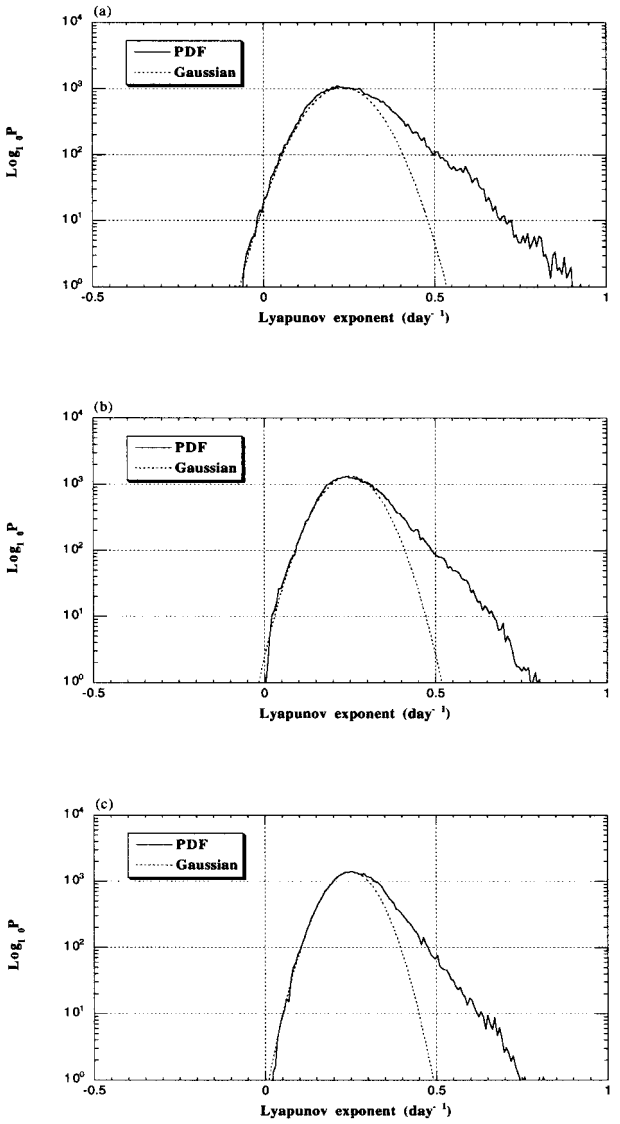

FIG. 2. The PDF of Lyapunov exponents. The 179 × 360 particles are initially arranged on 1° latitude–longitude grid (89.5°N to 89.5°S in latitude) on 1 Aug. The vertical axis is in logarithm. The PDF is calculated based on area weighting: (a) day 10, (b) day 20, (c) day 30.

the actual wind has weak divergence and convergence. These trajectories are of little consequence and become increasingly rare at longer times. By day 30, all the negative FTLEs have gone.

The most probable value of FTLEs is approximately 0.25 day^{-1}. This is a rather moderate value, smaller than that in the troposphere (Pierrehumbert and Yang 1993). If the dissipation scale were 100 km, for example, then according to the argument in section 2 the concentrations after 30 days of mixing are averages of samples of the initial data taken along filaments of length 180 000 km, which is only long enough to wrap around the globe about 5 times. Clearly, even apart from the limited meridional extent of filaments seen in Fig. 1, this length is not nearly enough to uniformly sample the initial tracer field. From this, we conclude that for most parts of the flow, 30 days is too short a time to put us very deeply into the asymptotic well-mixed regime. For 60 days mixing, the corresponding sampling filament is long enough to circle the earth more than 8700 times, and each parcel in the final state arises from a mixture of a more complete sampling of air from the initial condition. The problem remains, as indicated in Fig. 1, that the string of source air is meridionally confined, and samples air only from a narrow latitude band. There is no way of inferring this behavior from the FTLE distribution. It is a property of trajectory separation ''in the large,'' and is independent of the behavior of the FTLEs, which only measure the rate of separation of trajectories when they are close enough to each other for the trajectory problem to be linearized about the mean of the two trajectories.

The PDFs of Lyapunov exponent are Gaussian except for the appearance of an exponential high-stretch tail on the right-hand side, as seen in Fig. 2. Theory for homogeneous ergodic flows (Chertkov et al. 1995), without jets or barriers, does not account for the strongly non-Gaussian high-stretch tail. To identify the effects of the Tropics and the polar night jet, we have recomputed the Lyapunov exponent PDF for a surf-zone region alone.[2] These results are shown in Fig. 3. Compared with the PDF in Fig. 2, the PDFs in the surf zones have shorter exponential tails. In particular, the PDF in the southern surf zone (Fig. 3b) shows very weak departure from Gaussian. The low-stretch tail is still Gaussian, but its width is now such that low values of the FTLEs are far less probable than was the case for Fig. 2. Thus, the lowest FTLEs are preferentially found in the Tropics, while the largest ones are associated with the polar night jet.

Figure 4 quantifies the rate at which the PDF of FTLEs narrows with time. To measure the width, we fit each curve in Fig. 2 with a Gaussian $P(\lambda) \propto \exp[-(\lambda - \overline{\lambda})^2/2\sigma_\lambda^2]$, and plot how $2\sigma_\lambda$ depends on the length of time over which the Lyapunov exponent is computed. This curve can be approximately fitted by $2.55/\sqrt{t}$ (dotted curve) after about 7 days. This is precisely the result expected from an accumulation of the effects of random, independent strain, as derived by Chertkov et al. (1995). It is interesting that this behavior emerges despite the effectively nonergodic behavior of atmospheric flow, as manifest by the prominence of mixing barriers that constrain atmospheric transport. Evidently, trajectories do not stick to barrier regions long enough to affect the statistical convergence of the FTLE distribution as time

[2] Surf zone generally means winter midlatitudes where planetary waves break and lead to chaotic mixing (McIntyre and Palmer 1984). In the present paper, we refer to the summer midlatitudes as the summer ''surf zone'' since similar phenomena of wave breaking and tracer mixing are observed also in summer midlatitudes.

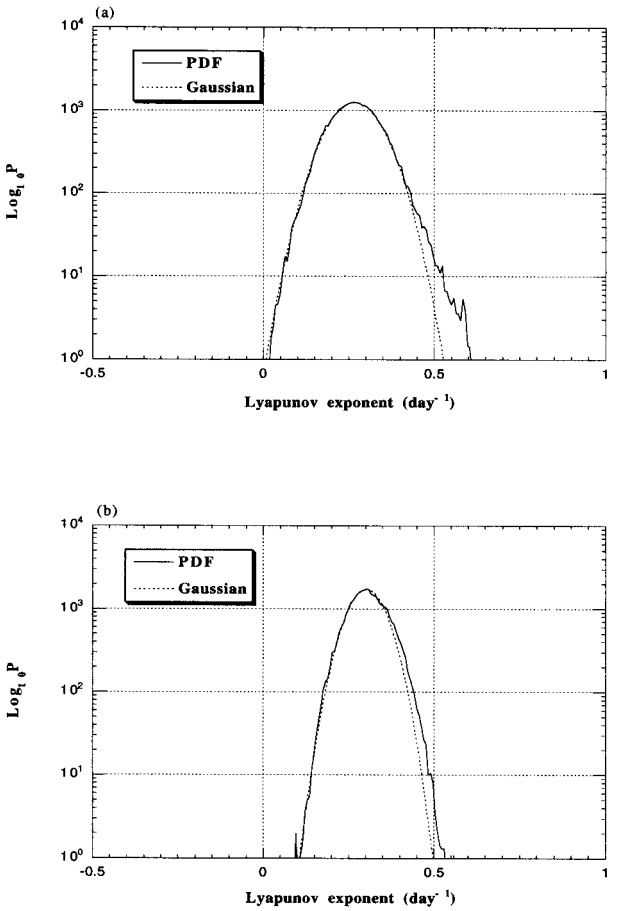

FIG. 3. The surf-zone PDFs of Lyapunov exponents on 30 Aug. (a) Northern surf zone, 90 × 360 particles are initially arranged in the band from 50° to 20°N; (b) southern surf zone, same amount of particles are arranged in the band from 20° to 50°S.

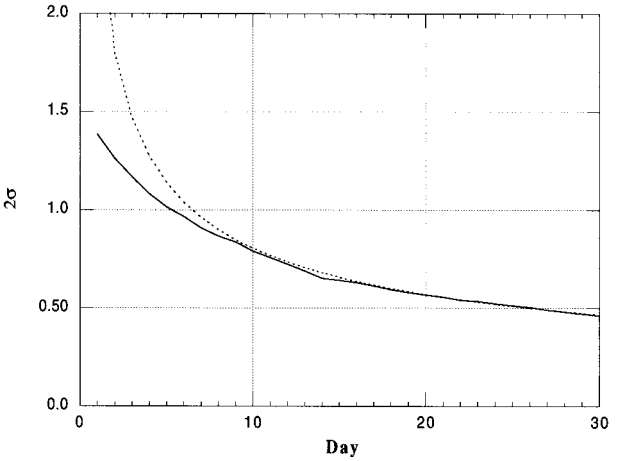

FIG. 4. The width ($2\sigma_\lambda$) of the PDF of Lyapunov exponents as a function of time.

progresses, or to cause the low-stretch tail to deviate from a Gaussian.

The general implication of the Lyapunov exponent behavior found above is that the nature of the PDFs of FTLEs for realistic flow is sufficiently in accord with that assumed in simplified theory of the tracer PDF [notably Chertkov et al. (1995)], that it presents no impediment to the applicability of the idealized theories. Significant non-Gaussian behavior is found only in the high-stretch tail, but this is of little consequence for the tracer PDF's, as the long-term behavior of the tracer is dominated by the *low-stretch* tail, which is Gaussian. The dominance of variability by the low-stretch tail also limits the importance of the rather broad spread of FTLEs found in the 30–60-day range. Shortcomings of the idealized theories have their roots elsewhere.

5. Characterization of basic mixing properties

Because of the presence of zonal jets, tracer mixing in the zonal direction proceeds very differently from mixing in the meridional direction. Apart from the diffusive effects that are the focus of the present study, the role of the jets is similar to that discussed for undiffused tropospheric flow by Pierrehumbert and Yang (1993), and gives the problem something of the flavor of shear-dispersion. In order to separately characterize along-jet and cross-jet mixing, we consider two classes of initial conditions. In the first, the initial tracer field varies only in the zonal direction, while in the second it varies only with latitude. The former case will be referred to as ''zonal mixing,'' and the latter as ''meridional mixing.''

a. Zonal mixing

In Fig. 5 we show the evolution of the initial condition $\theta_0 = \cos(2x)$, where x is longitude, for July–August 1992.

Already during the first 10 days, the tracer field has developed a great deal of small-scale structure. Figure 5b exhibits the typical features of chaotic mixing. Memory of the initial condition has been largely lost. Some tracer parcels are stretched into long and thin filaments, as expected from the positive FTLEs. Some filaments are folded into spiral structures. By day 20 (Fig. 5c), the tracer field has been further homogenized. In most parts of the Southern Hemisphere, the concentration approaches its mean value. Vortex structures can be seen near the North Pole. Extreme concentrations still exist in the form of unmixed filaments in the northern extratropics and subtropics. Some trapped structures are mainly located in the Tropics. Here, the trapped structures imply that some tracer blobs in the Tropics remain unmixed and have little change of their shape though they move along the mean tropical flow. These trapped structures in the tropics are quite persistent and still can be seen even after 60 days (Fig. 5d).

The tracer mixing proceeds differently in the Northern and Southern Hemispheres. In the Southern (winter) Hemisphere the tracer is more homogeneous and more zonally oriented. In contrast, the tracer field in the

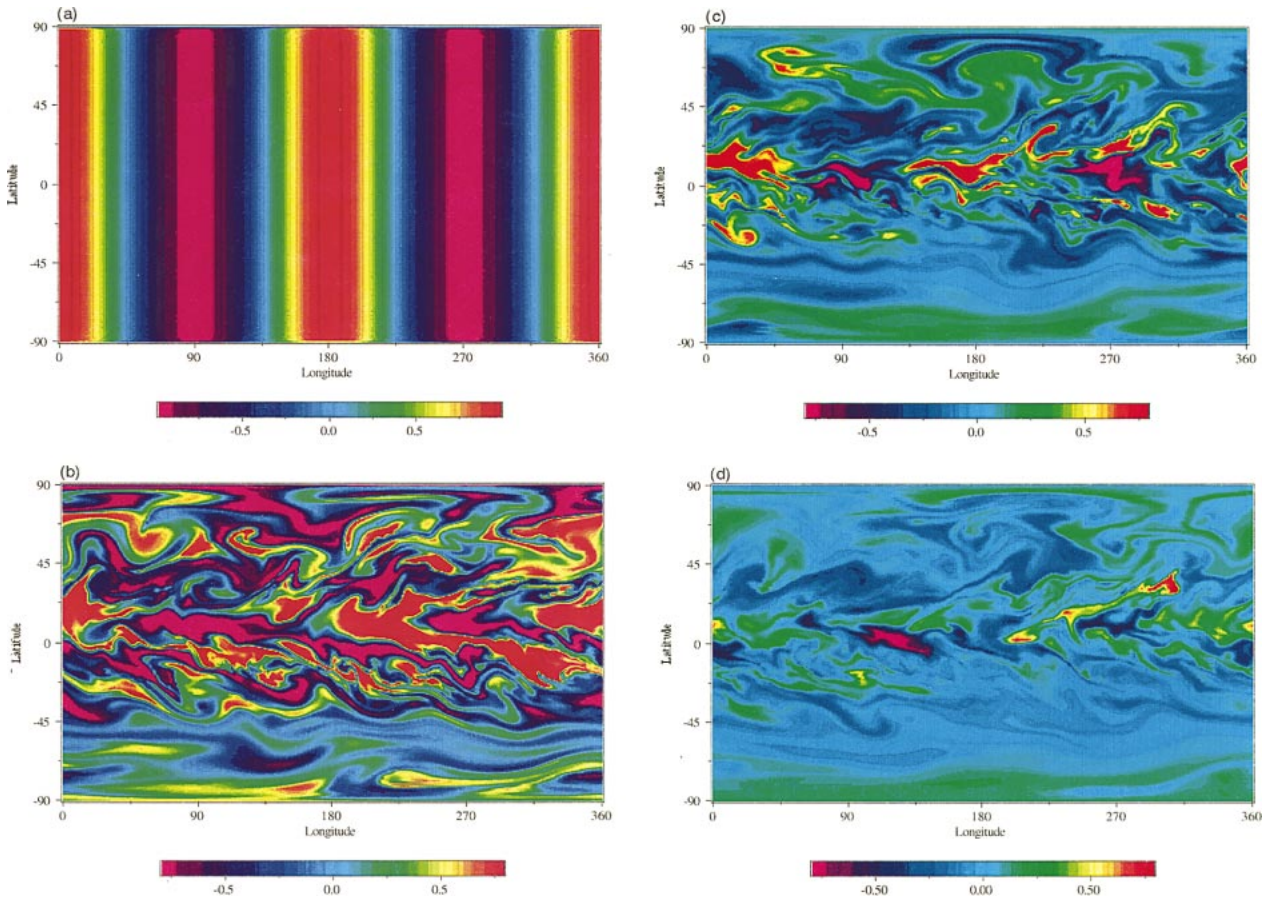

FIG. 5. Snapshots of zonal mixing. In order to clarify the small-scale structures, color scales are not same, but marked in color bars. (a) Day 0 (1 Jul), initial condition $\theta_0 = \cos(2x)$; (b) day 20; (c) day 40; (d) day 60.

Northern (summer) Hemisphere is less well mixed, and there are more trapped structures and large fluctuations. The asymmetric mixing is due to the difference in planetary wave activities and zonal shear strength. The winter hemisphere westerly winds are stronger and allow more wave propagation upward into the lower stratosphere from lower levels. The asymmetric mixing is also consistent with the difference of FTLEs between the two hemispheres shown in Fig. 3; that is, the FTLEs in the Northern Hemisphere are on the average smaller than those in the Southern Hemisphere.

The tropical trapped structures, with more negative concentrations, are due to the tropical weak-mixing zone where both wind shear and wave activity are quite weak. This feature of tropical trapped structures was also found by Pierrehumbert and Yang (1993) in particle trajectory calculations in the troposphere. Note that our result does not mean that the Tropics preferentially traps low concentrations. The preferential appearance of low concentrations in the Tropics is an artifact of the phase of the initial condition. It so happens that the concentration values which overlap the zonal locations of weakest tropical mixing are low values. For example, if the initial condition were $\sin(2x)$, rather than $\cos(2x)$, one would see more trapped structures with positive concentrations. Note that due to the lack of geostrophic balance in the Tropics the analyzed tropical winds are not so reliable as that in higher latitudes. But the weak-mixing behavior, resulting from the winds, is roughly reasonable.

In Fig. 6 we plot the decay of tracer fluctuation moments (order 1 to 5) over time corresponding to Fig. 5. Note that the vertical axis is logarithmic. Let us first look at the decay of the second-order moment, that is, tracer variance. It displays all the classic features familiar from simpler models of advection–diffusion by flows with dominantly positive Lyapunov exponents, discussed in Pierrehumbert (1994, 2000) and Antonsen et al. (1996). There is an initial brief period of no decay, during which tracer variance is being cascaded down to a scale sufficiently small for diffusion to be effective. Thereafter the variance decays exponentially in time at a rate that is on the order of the most probable Lyapunov exponents. The emergence of an exponentially decaying ''strange eigenmode'' in chaotic advection–diffusion was first predicted in Pierrehumbert (1994), and the phenomenon has recently been experimentally confirmed by Rothstein et al. (1999).

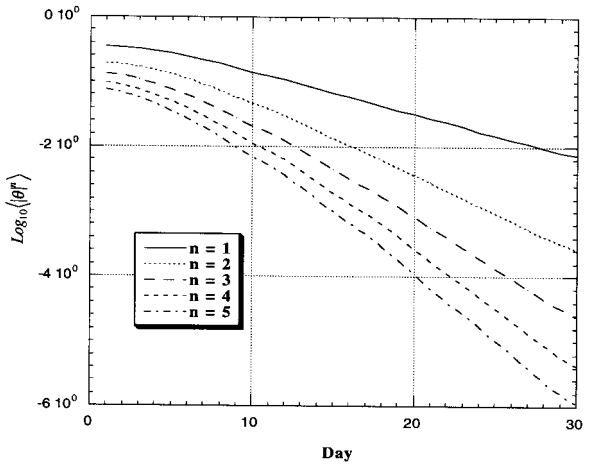

FIG. 6. Decay of tracer moments with time in the case of zonal mixing.

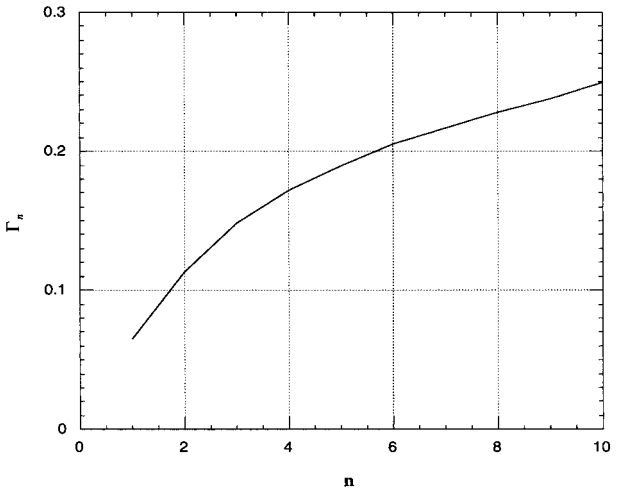

FIG. 7. Decay rates of tracer moments as a function of moment order.

Like the variance decay, all the other moments also decay exponentially with time, that is,

$$\langle |\theta|^n \rangle \propto \exp(-\Gamma_n t), \tag{8}$$

where Γ_n is the decay rate of the n^{th} moment of θ. A common assumption for the decaying case is that the shape of the PDF is time invariant, once the abscissa is rescaled according to the decaying tracer standard deviation (Sinai and Yakhot 1989; Yakhot et al. 1990). In this case $P(\theta, t) = f(\theta/\sigma_\theta(t))/\sigma_\theta(t)$, where σ_θ is the standard deviation of θ and f is some function. With this self-similar form of P, the moment decay rates would be characterized by $\Gamma_n \propto n$. Fig. 7 shows that the increase of Γ_n is clearly slower than linear, however. Thus, the assumption of a self-similar PDF is clearly inappropriate over the timescales of present consideration. The flattening of the Γ_n at large n in Fig. 7 indicates that the probability of extreme concentration fluctuations decays more slowly in time than would be expected on the basis of a self-similar collapse of the PDF.

The time evolution of the PDF, and its deviation from Gaussianity, can be characterized by the flatness. The flatness is

$$F(t) = \frac{\langle |\theta|^4 \rangle}{\langle |\theta|^2 \rangle^2} \propto \exp[-(\Gamma_4 - 2\Gamma_2)t]. \tag{9}$$

From Fig. 6, we can calculate the decay rates $2\Gamma_2 \approx 0.1$ and $\Gamma_4 \approx 0.07$. From this we obtain the flatness

$$F(t) \propto \exp(0.03t), \tag{10}$$

which grows exponentially with time. This implies that the tracer field becomes more and more intermittent with time, in the sense that extreme events become progressively more prominent. Recall that a Gaussian PDF has flatness $F = 3$. According to Eq. (10), non-Gaussian tails will occur after about day 35 even if the initial flatness is as small as unity, corresponding to an initial PDF that has steeper tails tha a Gaussian. For the zonal mixing case, at day 30, $F = 6.18$. This is close to the flatness of an exponential distribution, 6. Very long time integrations with idealized flows have shown stretched exponential tails, which are even more slowly decaying than the exponential distribution (Pierrehumbert 2000). The straightforward evolution toward a fixed, large flatness at longer times is not found in our case. For the zonal mixing case, the PDF over very long timescales is of little practical interest. First, when the integrations for the zonal mixing case are extended to 60 days or beyond, the evolution becomes dominated by remaining meridional gradients, and the evolution begins to resemble the meridional mixing case discussed below. Second, cross-isentropic diabatic mixing becomes nonnegligible as the length of integration extends beyond 2 months.

The evolution of the PDF of tracer fluctuations is shown in Fig. 8. The PDF of the initial distribution is strongly peaked at the extreme concentration values (Fig. 8a). This initial PDF corresponds to the initial condition $\theta_0 = \cos(2x)$. Note that the horizontal axis has been normalized by the root-mean-square (rms) of tracer fluctuations θ'_{rms}, where $\theta' = \theta - \langle\theta\rangle$, and $\theta'_{\text{rms}} = [\langle\theta'^2\rangle]^{1/2}$. After 20 days (Fig. 8b), the mixing has blended positive and negative values and the peak has shifted to $\theta'/\theta'_{\text{rms}} = 0$, though the range of concentration values is still broad. By day 40 (Fig. 8c), the PDF has taken on a shape with a Gaussian core near $\theta'/\theta'_{\text{rms}} = -0.5$ and two exponential tails. This shape does not change very much after day 40. The Gaussian core corresponds to the almost homogeneous part of the tracer field in Fig. 5, mostly in midlatitudes, while the exponential tails arise primarily from trajectories having low FTLEs, such as the trapped structures in the Tropics. The numerical results in Pierrehumbert (2000) indicate a stretched exponential tail at long times, which is even more slowly decaying than an exponential, indicating

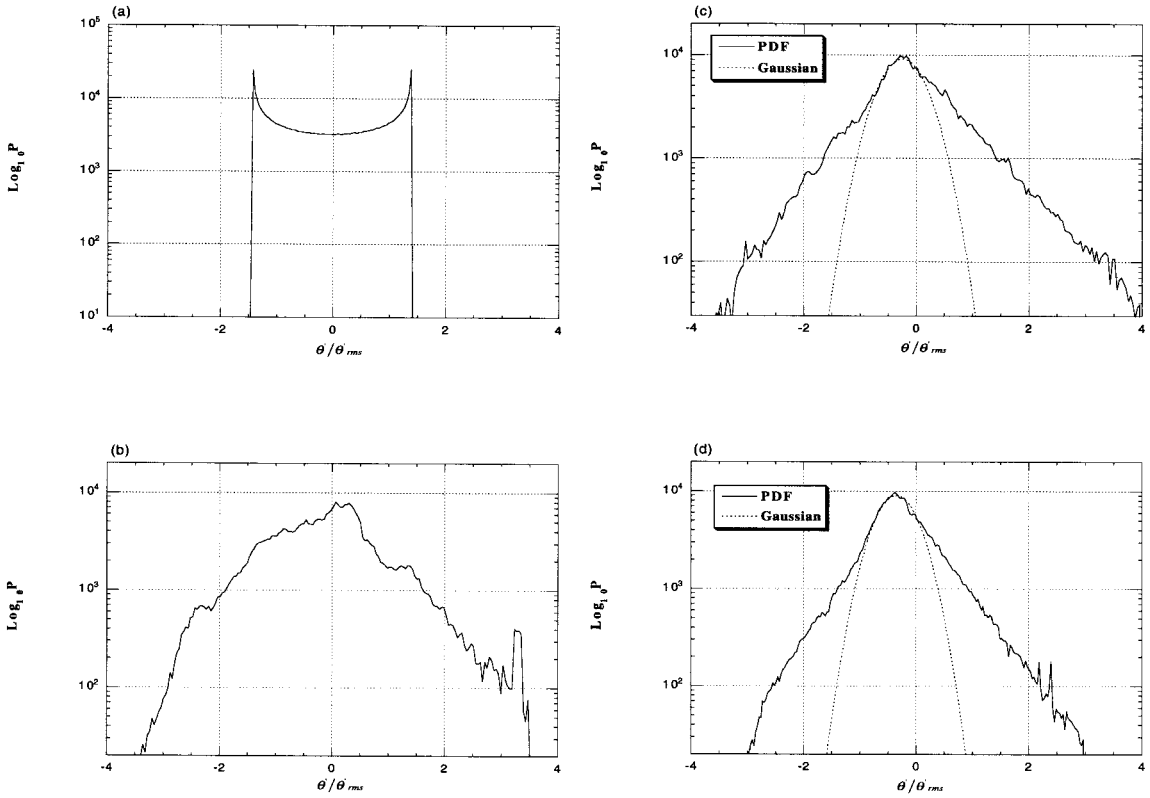

FIG. 8. The PDF of tracer fluctuations for the case of zonal mixing. The dotted line is a Gaussian fitting curve that indicates the Gaussian core of the PDF on 30 Aug. The vertical axis is in logarithm, and the horizontal axis is normalized by the root-mean-square of tracer fluctuations, $\theta'/\theta'_{\text{rms}}$. The tracer PDFs are all calculated based on area weighting: (a) day 0 (1 Jul), (b) day 20, (c) day 40, (d) day 60.

that the precise form of the tail depends on the nature of the flow and perhaps also the length of time the tracer is allowed to decay, with purely exponential tails tending to occur at a fairly early stage in the decay process.

From the tracer patterns (Fig. 5), we have found that tracer mixing proceeds differently in the Northern and Southern Hemispheres. In order to distinguish the difference in terms of PDFs, we plot the PDFs for the northern and southern surf zones (20°–50°N and 20°–50°S, respectively) in Fig. 9. The obvious difference between the two surf-zone PDFs is that the one in the Northern Hemisphere (Fig. 9a) has a broader distribution than the one in the Southern Hemisphere (Fig. 9b). This is consistent with what we saw in the mixing map that shows more prevalent and stronger tracer fluctuations in the Northern Hemisphere. The strong asymmetry of the two PDFs, and bias toward negative fluctuations, is associated with the preferentially, weakly mixed tracers marked with predominantly negative tracer values (cf. the dark-blue areas in midlatitudes in Fig. 5d).

The difference of the surf-zone tracer PDFs is also consistent with the Lyapunov exponent PDFs in surf zones. We have discussed in section 4 that the tails of a tracer PDF are determined by small FTLEs, that is, the left tail of the FTLE PDF. From Fig. 3, we observe that the left tail of the Lyapunov exponent PDF in the northern surf zone (Fig. 3a) consists of much smaller FTLEs compared with that in the southern surf zone (Fig. 3b). This means that it is the small FTLEs that lead to large tracer fluctuations and broad exponential tails. Additionally, the fact that the Lyapunov exponent distribution is narrower for the southern surf zone than that for the northern surf zone is consistent with the more prominent Gaussian core in the PDF of θ in the south. Thus, comparison of the surf-zone tracer PDFs with the Lyapunov exponent PDFs further illustrates the dependence of tracer statistics on Lyapunov exponent statistics.

To examine the effect of resolution on the tracer fluctuations, we have carried out a zonal mixing calculation at reduced resolution. As expected from theory, the tracer standard deviation after 60 days is reduced, but the shape of the PDF (not shown) is left unchanged. Specifically, in reducing the resolution from 30 to 120 km, the rms tracer fluctuation after 60 days is reduced from 0.390 to 0.187, from which we can estimate the flow-dependent exponent in (4). It appears that the rms tracer fluctuation at a fixed time increases in inverse proportion to the square root of the grid size.

Figure 10 shows the conditional diffusion (Fig. 10a) and dissipation (Fig. 10b) on 30 August for the zonal

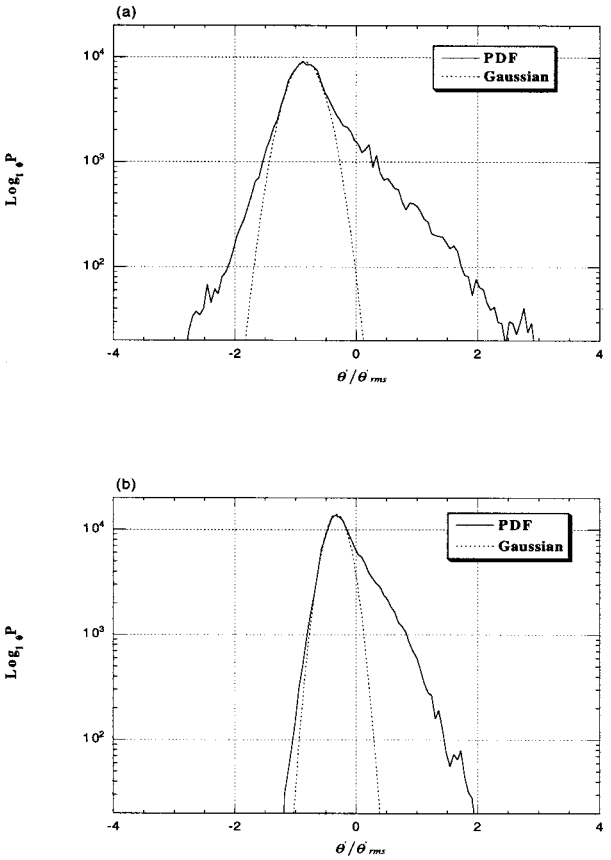

FIG. 9. The surf-zone PDFs of tracer fluctuations on 30 Aug. The PDFs are calculated in the same domains as in Fig. 3 and normalized using the global $\theta'_{\rm rms}$. (a) Northern surf zone, (b) southern surf zone.

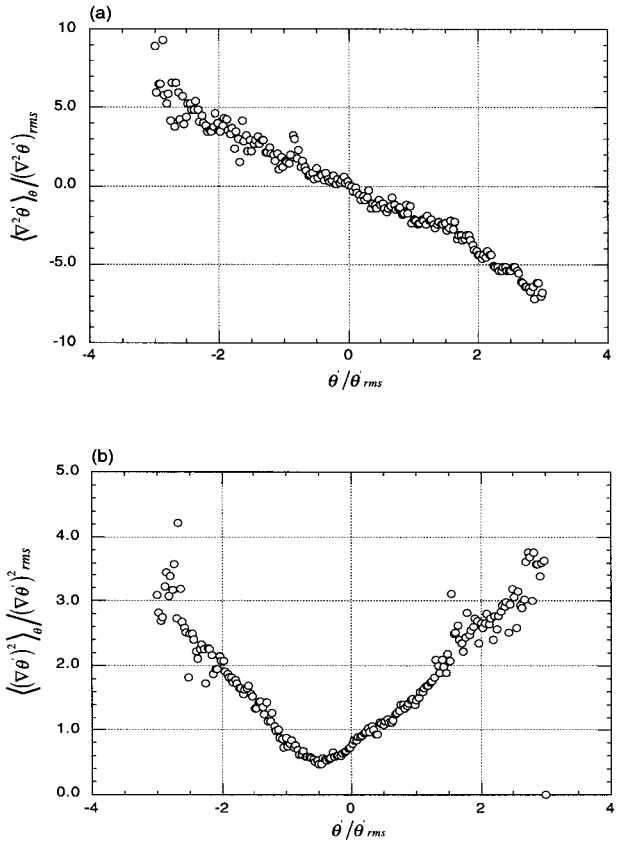

FIG. 10. (a) Conditional diffusion, 30 Aug. (b) Conditional dissipation, 30 Aug.

mixing case. The conditional diffusion is nearly linear in θ, and implies a constant mean decay rate of tracer fluctuations. A linear conditional diffusion was also observed in laboratory experiments (Pope and Ching 1993), the idealized decaying tracer simulations of Pierrehumbert (2000), and a variety of other idealized mixing simulations by Ngan and Pierrehumbert (2000).

Also in common with idealized decaying tracer cases, the conditional dissipation shows a flat minimum as $\theta \to 0$ and increases monotonically with increasing magnitude of the tracer fluctuation relative to its mean value. Unlike the idealized cases in Pierrehumbert (2000), the increase for the case shown is linear in fluctuation, rather than quadratic. We do not yet have any explanation for this difference. The range of variation of the conditional dissipation is pronounced; it increases by a factor of 4 or more between its minimum value and its value at the 2 standard deviation tracer fluctuation. This implies substantial deviations from Gaussian behavior, with tails that are considerably more probable than Gaussian.

We can quantify the implied deviation from Gaussianity using the Ching–Kraichnan formula. Based on Fig. 10, we assume

$$\langle \nabla^2\theta \rangle_\theta = -k\theta, \qquad \langle |\nabla\theta|^2 \rangle_\theta = a + b|\theta|. \quad (11)$$

Then, Eq. (7) can be evaluated analytically. In the limit $\theta \to 0$,

$$P(\theta) \propto \exp\left(-\frac{k}{2a}\theta^2\right), \quad (12)$$

which is Gaussian. As θ becomes large,

$$P(\theta) \propto \frac{C_1}{b|\theta|}\exp\left(-\frac{k}{b}|\theta|\right), \quad (13)$$

which is close to exponential. This suggests a crossover solution matching the core and tails of $P(\theta)$:

$$P(\theta) \propto \frac{C_1}{a + b|\theta|}\exp\left(-\frac{k\theta^2}{2a + b}|\theta|\right). \quad (14)$$

The crossover from Gaussian to exponential behavior occurs near $|\theta| = 2a/b$. These results are consistent with the PDF's in Figs. 8c and 8d. In contrast, a quadratic form of conditional dissipation as shown in Pierrehumbert (2000) yields the Sinai–Yakhot shape of tracer PDF with algebraic tails, which are even much flatter than exponential.

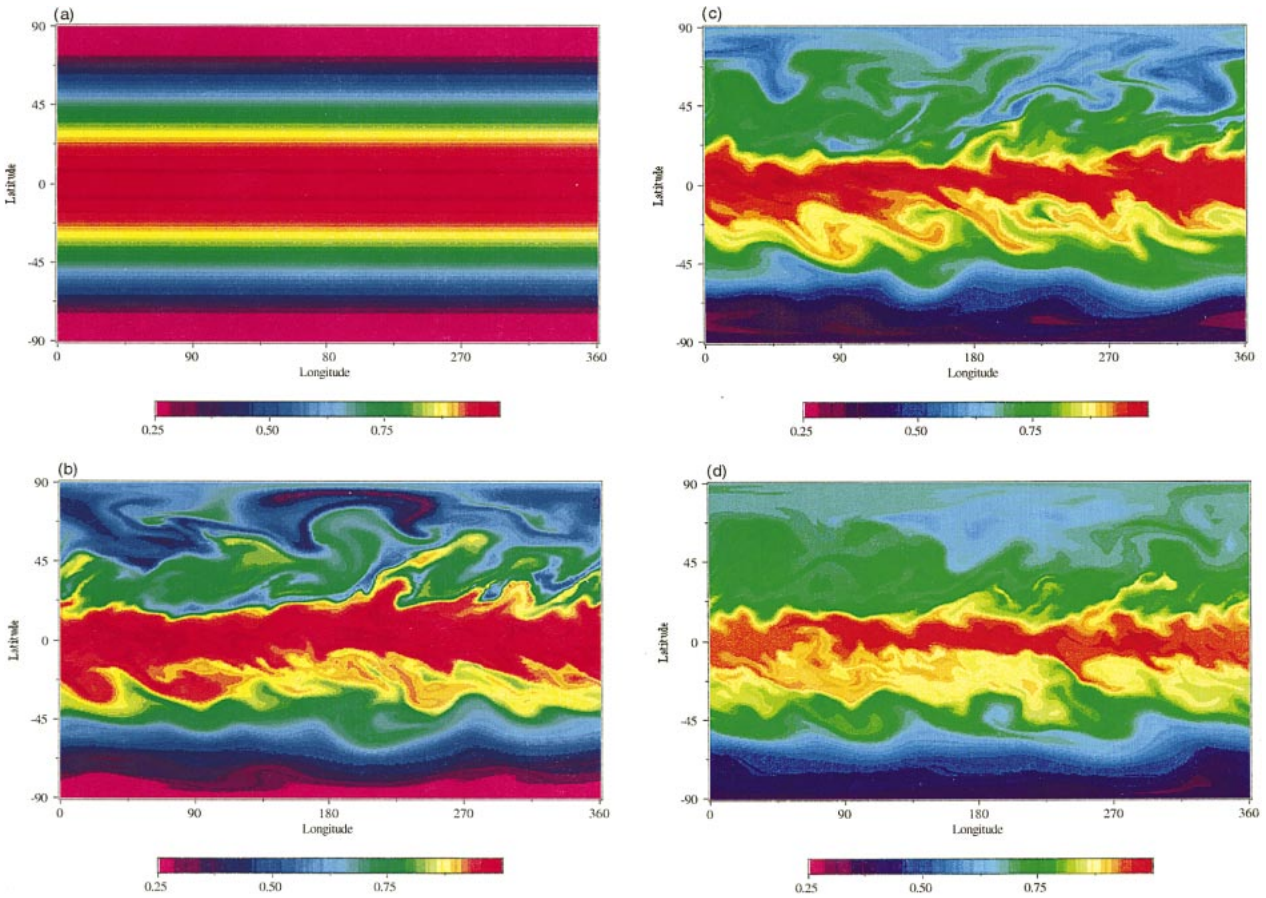

FIG. 11. Snapshots for meridional mixing: (a) day 0 (1 Jul), initial condition $\theta_0 = \cos(y)$; (b) day 20; (c) day 40; (d) day 60.

b. *Meridional mixing*

In Fig. 11 we show the evolution of the initial tracer field $\theta_0 = \cos(y)$, under advection by the flow of July–August, 1992, where y indicates latitude. The essential feature to note is that there is substantial mixing within narrow latitude bands, but that the mixing is unable to appreciably reduce the mean global gradient even after 60 days. The globe is carved up into a number of mixing zones, separated by mixing barriers which in some cases are rather permeable and in other cases are nearly absolute. The mixing barriers between Tropics and extratropics are rather permeable, as witness the erosion of the red (tropical) band in Fig. 11. Likewise, there is fairly good mixing throughout the Northern (summer) Hemisphere extratropical to polar zone. In contrast, the mixing barrier bounding the winter Antarctic polar vortex is nearly perfect. There is a good deal of mixing within the Antarctic polar vortex, but mixing across the barrier, marked by light blue air located between 60° and 70°S, is nearly absent. Because the global-scale meridional gradient remains nearly intact, the global tracer variance hardly decays at all (see Fig. 12).

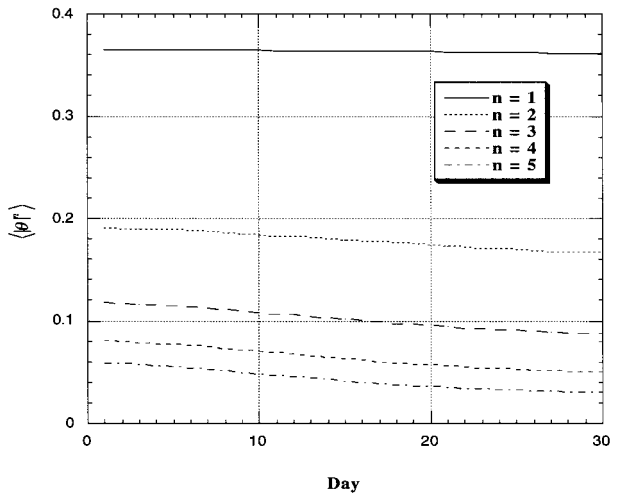

FIG. 12. Decay tracer moments with time in meridional mixing. Note that in this case the vertical axis is linear.

The tropical region is a repository of relatively unmixed high tracer values, which intermittently eject filaments into the surf zones. The effect of the Antarctic polar mixing barrier is like a solid boundary, while the effect of the tropical barriers is similar to the effect of the bottom wall in the Rayleigh–Bénard convection ex-

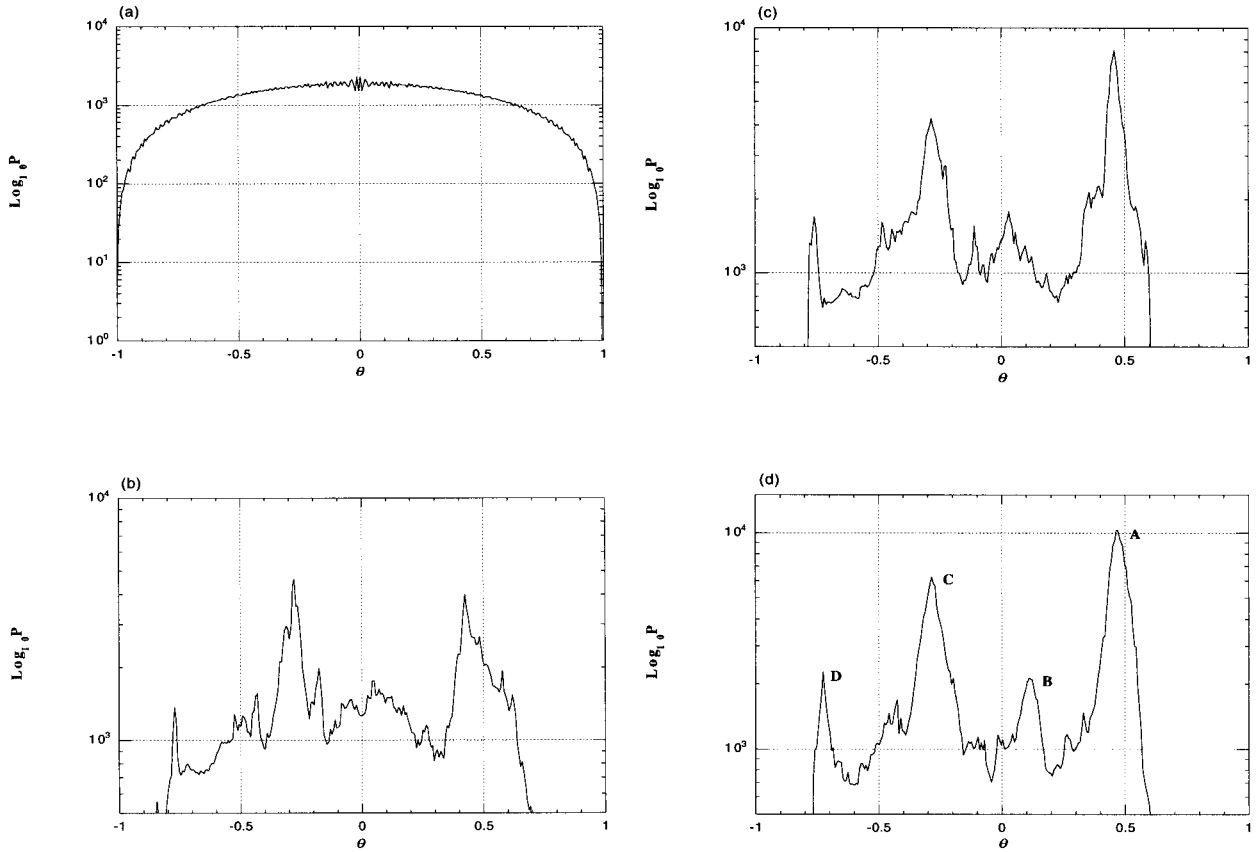

FIG. 13. The PDF of tracer fluctuations for meridional mixing. In this case, the initial condition is $\theta_0 = y/90.0$. Note that the horizontal axis is not normalized: (a) day 0 (1 Jul), (b) day 20, (c) day 40, (d) day 60.

periment (Castaing et al. 1989), through which buoyancy forcing from the bottom wall produces anomalous temperature fluctuations.

The confinement of mixing to distinct meridionally limited zones shows up also in the PDF of global tracer concentrations. In order to distinguish Northern Hemisphere from Southern Hemisphere mixing, we evaluated the PDFs for the initial condition $\theta_0 = y/90$ (y is latitude in degrees), in place of the symmetric initial condition chosen previously in order to best highlight the tracer pattern. The evolution of the global PDF is shown in Fig. 13. Rather than collapsing onto a single peak, the PDF is multimodal, with one peak corresponding to each mixing zone. In fact, with the initial condition we have chosen, the concentration value at which each peak occurs marks the latitude of the center of the corresponding mixing zone. A calculation of this sort therefore serves as a quick and simple way to locate the major mixing barriers of a flow. In this case, there are four mixing zones: the northern polar extratropics (peak A), the tropical weak-mixing zone (peak B), the southern surf zone (peak C), and the Antarctic polar vortex (peak D). These peaks are sandwiched by mixing barriers. After 60 days, concentration values have become somewhat homogenized within each mixing zone. Mixing between the zones procedes much more slowly, if at all. Note that peak B is at the positive side of θ, rather than around $\theta = 0$. This is consistent with Fig. 11d, which shows that the tropical weak-mixing zone is located at the northern (summer) side of the equator.

In order to better characterize the PDFs within each mixing zone, we subtracted off the slowly varying zonal mean of the tracer field, and computed PDFs for the tracer deviation within various latitude bands. The concentration fluctuations are normalized by the root-mean-square average of the *global* tracer fluctuation field. Results on 30 August are shown in Fig. 14. Both the northern and southern surf zone regions show a small Gaussian core and pronounced exponential tails. Most part of the PDF curve in the tropical region, on the other hand, can be fit by Gaussian. The typical tracer fluctuation in this region has roughly twice the magnitude as for the southern surf zone, consistently with the weak mixing in the deep Tropics. The broad Gaussian core in the Tropics probably arises because the mixing here is still at a fairly early stage in its development. The fundamental timescale is provided by the dominant Lyapunov exponent, which is small in the Tropics. Experience with simple models (Pierrehumbert 2000) indicates that early-stage mixing rapidly yields a broad Gaussian core,

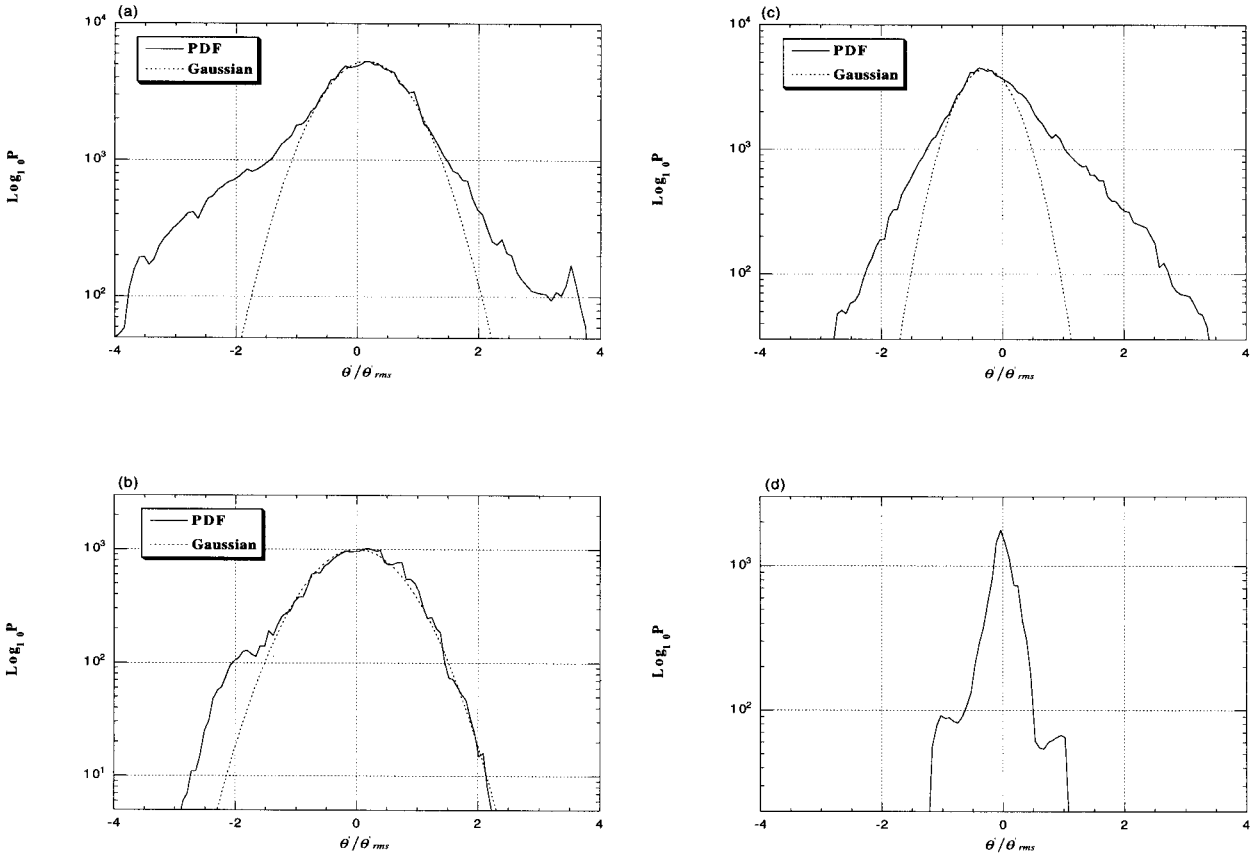

FIG. 14. Regional PDFs for meridional mixing, 30 Aug. The normalized PDFs are calculated in different regions. (a) Northern surf zone (50°–20°N), (b) Tropics (10°N–10°S), (c) southern surf zone (20°–50°S), (d) Antarctic (70°–90°S).

which gradually develops fatter tails as the ''typical'' regions decay rapidly and leave behind the more slowly decaying and rarer extreme fluctuations. The PDF in the Antarctic region appears noisy, owing to the small number of effective degrees of freedom in the polar region. Insofar as a characteristic shape can be discerned, the tails are even fatter than exponential, and there is some suggestion of stretched-exponential behavior as in the late stage decaying results in Pierrehumbert (2000).

The conditional diffusion and dissipation of the tracer fluctuation field are shown for the northern and southern surf zones in Figs. 15 and 16. In both cases, the conditional diffusion is linear in the tracer fluctuation. The linearity of the conditional diffusion indicates that the tracer variability within each mixing region decays exponentially in the mean, even though the global total tracer variance is not significantly decaying. The slope of the conditional diffusion gives the local decay rate. Hence, a comparison of the two figures indicates that tracer fluctuations in the southern surf zone are decaying at about a third of the rate of those in the northern surf zone. As discussed before, the strong asymmetry in Fig. 15b is due nonhomogeneous and anisotropic mixing in the Northern Hemisphere where large negative fluctuations are preferentially found.

Given the linearity of the conditional diffusion, deviations from Gaussianity are entirely characterized by the conditional dissipation. In both surf zones, the conditional dissipation of tracer fluctuation increases linearly with the magnitude of the fluctuation, much as for the zonal decay case. The results imply exponential tails, as for the zonal case. Taken together, the conditional statistics and the PDFs indicate that, viewed locally, the processes governing the evolution of the deviation of tracers from their zonal mean are essentially the same as those appearing in the zonal mixing case.

The regionality of the mixing is a consequence of the presence of mixing barriers. In order to test the robustness of these barriers, we have conducted a run in which the winds are modified by artificially increasing the amplitude of the deviation of the winds from the zonal mean by a factor of 4, while keeping the zonal mean wind fixed. This process increases the ability of the winds to mix across jets. The same technique has been used by Bowman and Hu (1997) to break mixing barriers. Since the modified winds do not satisfy dynamical equations of motion, this experiment also serves to test the importance of dynamical constraints on the wind field, in determining the presence of barriers. The global PDFs are shown in Fig. 17. It is seen that the

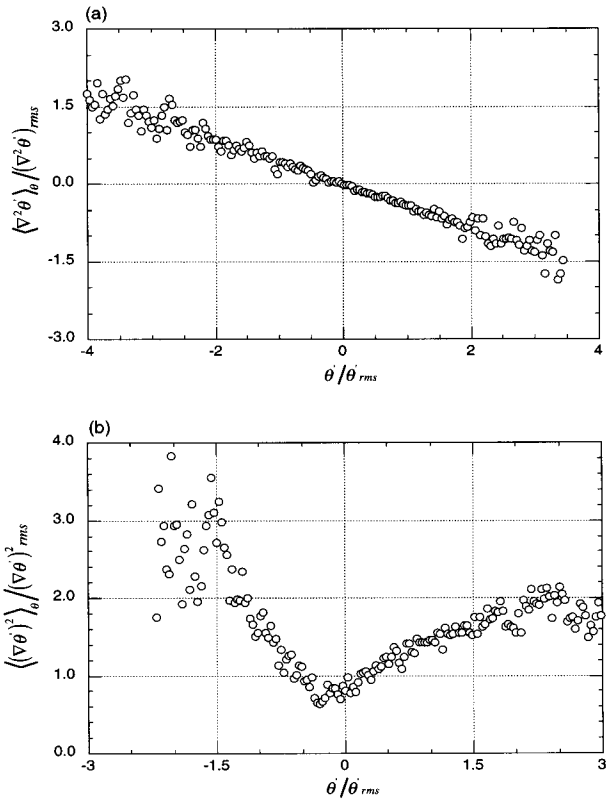

FIG. 15. Conditional diffusion and dissipation in the northern surf zone (50°–20°N). (a) Conditional diffusion, (b) conditional dissipation.

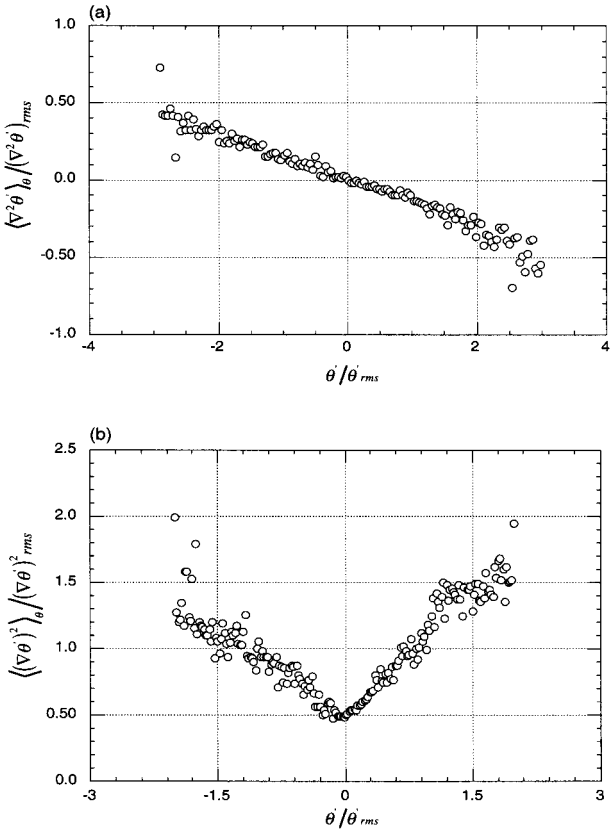

FIG. 16. Conditional diffusion and dissipation in the southern surf zone (20°–50°S). (a) Conditional diffusion, (b) conditional dissipation.

principal difference is that peak B merges into A, indicating the breaking of the winter (evidently weak) tropical mixing barrier. Peaks C and D survive, indicating a robustness of the corresponding mixing barriers. These barriers are evidently kinematic rather than dynamical in origin; they may depend on the generic streamline geometry, but they evidently do not rely on the wind field satisfying fluid dynamical equations. The broadening of the PDFs when mixing is enhanced is precisely opposite to what one would expect in the absence of mixing barriers. Without mixing barriers, enhancing mixing would lead to narrower PDFs, since enhanced mixing speeds homogenization. Homogenization is reflected in PDFs as a collapse onto a spike at the unique concentration value corresponding to the homogenized state. In the meridional case, enhanced mixing broadens the PDFs by enhancing the range of concentration values that can be blended within each mixing zone.

Although the experiment we have described is freely decaying, the preservation of the global meridional gradient makes the behavior similar to a forced-equilibrium case in which a mean gradient is maintained by forcing. In our case, the meridional gradient may eventually disappear, but until it does, it provides a continuing source of tracer fluctuations, associated with rare events that transport air over long meridional distances. The situation is thus qualitatively similar to that of stratospheric N_2O, since the tropical N_2O is kept high by upward mixing of high N_2O air from the troposphere, while high-latitude N_2O is kept low by advection of photochemically cleansed low N_2O air from aloft. One might thus expect N_2O to have similar PDFs to those seen in our meridional mixing experiment, in view of

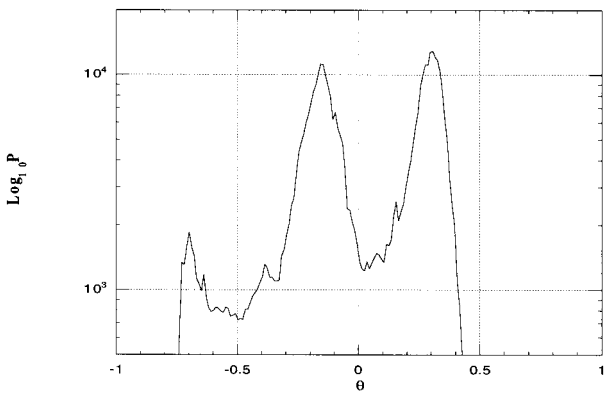

FIG. 17. Tracer PDF for meridional mixing with modified winds ($v \times 4$).

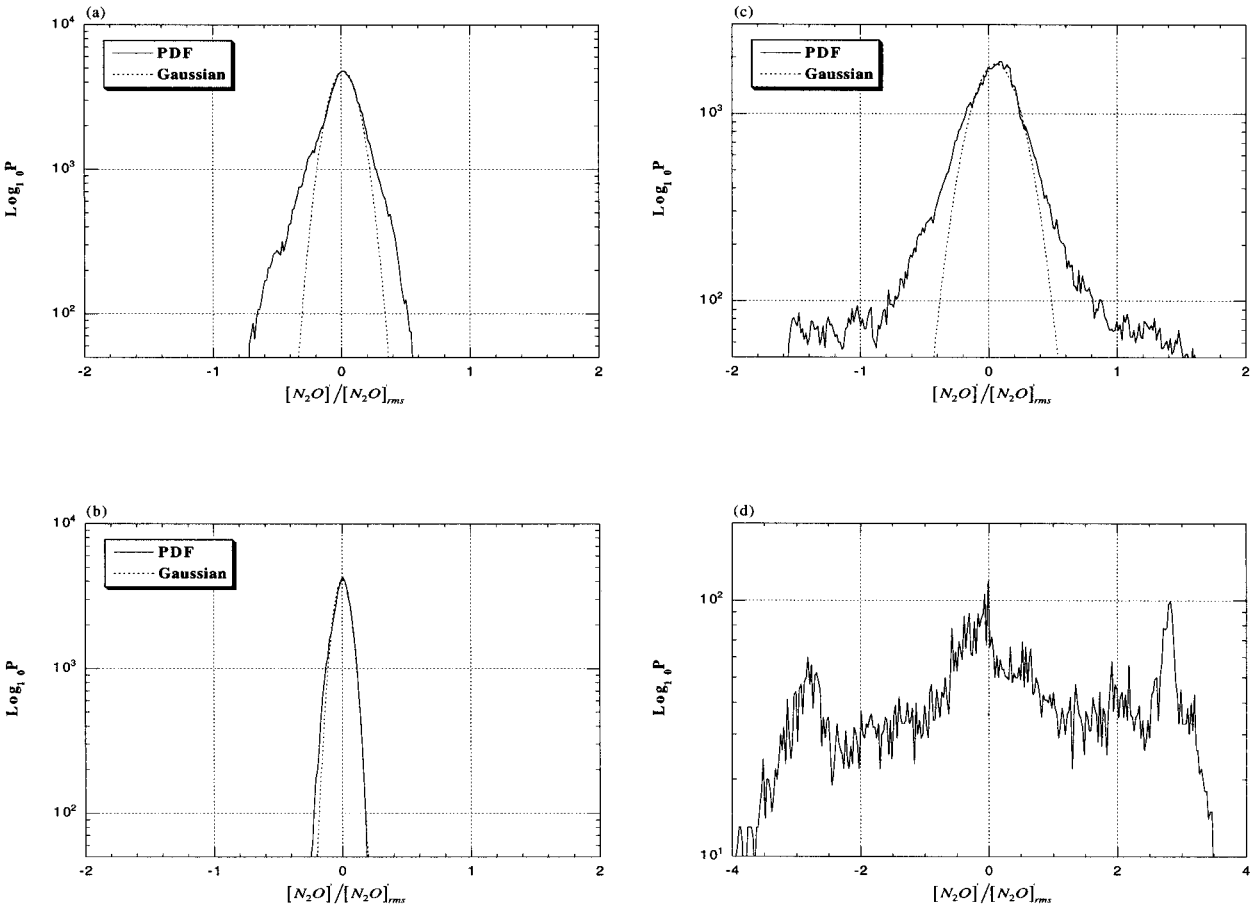

FIG. 18. Regional PDFs of N_2O in the SKYHI model. The PDFs were calculated in the same regions as that in Fig. 14. (a) Northern surf zone, (b) Tropics, (c) southern surf zone, (d) Antarctic.

the fact that N_2O is a long-lived tracer. In Fig. 18 we show the regional PDFs of N_2O on the 450 K isentropic surface in an August simulation carried out with the SKYHI stratospheric general circulation model [a description of the SKYHI model can be found in Hamilton et al. (1995), and N_2O mixing in the SKYHI model was discussed in Nakamura (1996)]. As with the regional PDFs in the decaying tracer case, we deal with the PDFs of the deviation of N_2O from its zonal mean, and normalize by the global rms average of the fluctuation. The PDFs were computed for the same regions as used in the idealized mixing case analyzed in Fig. 14.

The tropical PDF is very narrow, owing to the uniformity of the source air. The weak fluctuations there are well fit by a Gaussian distribution. Mixing of the tropical air with polar low N_2O air gives rise to a distribution of air with intermediate concentrations in the surf zones. Both the northern (Fig. 18a) and southern (Fig. 18c) midlatitude regions show a Gaussian core and exponential tails, as in the corresponding tracer-decay simulations shown in Figs. 14a and 14c, and the northern N_2O PDF even shows some signs of the same asymmetry seen in the tracer decay case. However, the idealized simulation does not capture the fact that the northern N_2O PDF is markedly narrower than the southern one, nor does it reproduce the broad, flat tails seen in the southern distribution at very extreme N_2O values. The N_2O PDF in the Antarctic polar vortex is broad and noisy, and bears little resemblance to the idealized tracer results.

In section 2, we have argued that the PDF shape is independent of diffusivity. The appearance of exponential tails of N_2O fluctuations in the SKYHI model supports this argument, since the SKYHI model has much lower resolution, $1° \times 1.25°$ in latitude and longitude, than that of our model.

6. Conclusions

We have shown that concepts arising from theoretical study of highly idealized fluid mixing situations have considerably utility in understanding the fluctuations of a long-lived tracer mixed by realistic stratospheric flow. A robust feature is the appearance of a Gaussian core in the probability distribution of small tracer fluctuations, with non-Gaussian ''fat tails'' of large fluctua-

tions. The fat tails are a consequence of populations of tracer that have experienced anomalously weak mixing, but are independent of the large-scale initial tracer condition. In the present case, the fat tails are generally exponential. The fat tails imply that for nonlinear chemistry large tracer fluctuations are important because these rare events have much higher probabilities than random events governed by Gaussian tails.

There is a marked difference between mixing of zonal variations of tracer and mixing of meridional variations. Zonal variations decay exponentially, giving rise to unimodal concentration PDFs. This is so because there are no barriers to zonal mixing.

Within the 2-month period, meridional variations do not homogenize globally. Rather, they homogenize within distinct mixing zones bounded by mixing barriers of varying permeability. This gives rise to a multimodal PDF, with one peak for each distinct mixing region. The computation of PDFs evolving from an initially meridional tracer gradient provides a convenient means for locating mixing barriers, and characterizing their permeability. Within each mixing zone, the character of the mixing is similar to the zonal mixing case, once one takes into account the limited range of concentration values that are being mixed. PDFs of stratospheric N_2O in the SKYHI general circulation model bear a strong resemblance to the PDFs appearing in our meridional mixing calculation, indicating that the N_2O are governed by advection–diffusion, and can be understood on the basis of generic properties of the advection–diffusion problem with underlying chaotic trajectories.

The probability distribution of finite-time FTLEs of the trajectory problem associated with the wind field provides a useful characterization of the key mixing properties, even though we are dealing with advection–diffusion rather pure advection. It is the low-stretch tail of the PDF of FTLEs that determines the rate at which tracer fluctuations decay and the prevalence of anomalously weak mixing giving rise to fat tails of the concentration PDF. The narrower the PDF of FTLEs, the more dominant is the Gaussian core of the concentration PDF. We emphasize that fat tails in the concentration PDF do not rely on non-Gaussian behavior of the FTLE PDF.

We have also demonstrated the utility of diagnosing the mixing in terms of the averages of diffusion and dissipation, conditioned on tracer concentration values. In both the meridional and zonal mixing cases, the conditional diffusion is linear in tracer value, indicating a mean exponential decay of local tracer fluctuations. The conditional dissipation is an average of a positive-definite quantity, and contains important information about the fluctuations in tracer decay rate. It is the conditional dissipation that characterizes the non-Gaussian behavior of the concentration PDF. In present case, the conditional dissipation is linear in the absolute value of concentration fluctuation, after a two-month model run; this leads to exponential tails in the concentration PDF.

Our results provide some insight as to the way in which diffusivity (a proxy for model resolution) affects the concentration PDF. For a large-scale initial condition, the time for the tracer to begin dissipating increases logarithmically with the inverse of the diffusivity, that is, increases logarithmically with increasing model resolution. After this initial transient adjustment time, the theoretical arguments and simulation results suggest that the PDF for the decaying tracer attains a resolution-independent asymptotic shape, though its overall width is resolution-dependent. Theory indicates that the root-mean-square tracer fluctuation at a fixed time should increase inversely with an order-unity power of the grid size. The expected increase was confirmed numerically for decay of zonal fluctuations, and the simulations suggest a square root power law. The resolution effect arises simply from the increase in mix-down time with resolution, which increases the delay before exponential decay sets in. The long-term exponential decay rate is not itself affected by resolution.

The resolution dependence for a tracer field maintained by sources and sinks may differ considerably from that of the freely decaying case we have studied. This is particularly likely when the sources and sinks of tracer are separated by a partial transport barrier, in which case the tracer variance is largely determined by the rate of leakage of tracer across the barrier. We suspect that the behavior of leakage through the polar vortex edge may account for much of the strong resolution effects on maximum Arctic active chlorine concentration, seen in Edouard et al. (1996). Active chlorine is also a rather short-lived tracer compared to characteristic mixing times, and so it could well be affected by resolution-dependent transient effects. These possibilities will be explored in future work, involving tracers maintained by sources and sinks, and ultimately tracers with finite lifetimes.

The use of PDFs provides a powerful diagnostic tool, a basis for comparing general circulation models with data, and a way for diagnosing the portion of errors that are due to errors in modeled circulations (via comparisons of the Lyapunov PDFs). Our results indicate that the PDFs in the decaying case contain little information about the nature of the small-scale dissipation, but that they do reflect information about the configuration of mixing regions, their permeability, and the Lagrangian mean strain rate of the advecting flow. Ultimately, the PDF methods may prove useful in developing parameterizations of the effect of subgrid tracer fluctuations on chemical reactions.

Acknowledgments. We thank S. Edouard for allowing us the use of her finite-volume code. Discussion with Keith Ngan, Misha Chertkov, and Eugeni Balkovsky has been very helpful in writing this paper. We are grateful to the three reviewers for their instructive comments. This project is supported by the ASCI Flash Center at The University of Chicago under DOE Contract

B341495, and by the National Science Foundation under Grant ATM9505190.

REFERENCES

Antonsen, T. M., Z. Fan, E. Ott, and E. Garcia-Lopez, 1996: The role of chaotic orbits in the determination of power spectra of passive scalars. *Phys. Fluids,* **8,** 3094–3104.

Balkovsky, E., and A. Fouxon, 1999: Universal long-time properties of Lagrangian statistics in Batchelor regime and their application to passive scalar problem. *Phys. Rev. E,* **60,** 4164–4174.

Batchelor, G. K., 1959: Small-scale variation of convected quantities like temperature in turbulent fluid. Part l, General discussion and the case of small conductivity. *J. Fluid Mech.,* **5,** 113–133.

Bowman, K. P., and Y. Hu, 1997: Tropical mixing barriers in the lower stratosphere in the Geophysical Fluid Dynamics Laboratory SKYHI model. *J. Geophys. Res.,* **102** (D17), 21 465–21 478.

Castaing, B., and Coauthors, 1989: Scaling of hard thermal turbulence in Rayleigh-Benard convection. *J. Fluid Mech.,* **204,** 1–30.

Chertkov, M., G. Falkovich, I. Kolokolov, and I. Lebedev, 1995: Statistics of a passive scalar advected by a large-scale two-dimensional velocity field: Analytic solution. *Phys. Rev. E,* **51,** 5609–5627.

Ching, E. S. C., and R. H. Kraichnan, 1998: Exact results for conditional means of a passive scalar in certain statistically homogeneous flows. *J. Stat. Phys.,* **93,** 787–795.

Edouard, S., B. Legras, F. Lefevre, and R. Eymard, 1996: The effect of small-scale inhomogeneities on ozone depletion in the Arctic. *Nature,* **384,** 444–447.

Eswaran, V., and S. B. Pope, 1988: Direct numerical simulations of the turbulent mixing of a passive scalar. *Phys. Fluids,* **31** (3), 506–520.

Gollub, J. P., J. Clarke, M. Gharib, B. Lane, and O. N. Mesquite, 1991: Fluctuations and transport in a stirred fluid with a mean gradient. *Phys. Rev. Lett.,* **67,** 3507–3510.

Hamilton, K. P., R. J. Wilson, J. D. Mahlman, and L. J. Umscheid, 1995: Climatology of the SKYHI troposphere-stratosphere-mesosphere general circulation model. *J. Atmos. Sci.,* **52,** 5–43.

Haynes, P. H., and J. Anglade, 1997: The vertical-scale cascade in atmospheric tracers due to large-scale differential advection. *J. Atmos. Sci.,* **54,** 1121–1136.

Jayesh, and Z. Warhaft, 1991: Probability distribution of a passive scalar in grid-generated turbulence. *Phys. Rev. Lett.,* **67,** 3503–3506.

Lumley, J. L., 1970: *Stochastic Tools in Turbulence.* Academic Press, 194 pp.

Majda, A. J., 1993: The random uniform shear layer: An explicit example of turbulent diffusion with broad tail probability distributions. *Phys. Fluids A,* **5,** 1963–1970.

——, and P. R. Kramer, 1999: Simplified models for turbulent diffusion: Theory, numerical modelling, and physical phenomena. *Phys. Rep.,* **314,** 237–574.

McIntyre, M. E., and T. N. Palmer, 1984: The ''surf zone'' in the stratosphere. *J. Atmos. Terr. Phys.,* **46,** 825–849.

Methven, J., and B. Hoskins, 1999: The advection of high-resolution tracers by low-resolution winds. *J. Atmos. Sci.,* **56,** 3262–3285.

Nakamura, N., 1996: Two-dimensional mixing, edge formation, and permeability diagnosed in an area coordinate. *J. Atmos. Sci.,* **53,** 1524–1537.

Ngan, K., and R. T. Pierrehumbert, 2000: Spatially inhomogeneous and intermittent random advection. *Phys. Fluids,* **12,** 822–834.

Peyret, R., and T. Taylor, 1983: *Computation Methods for Fluid Flow.* Springer-Verlag, 358 pp.

Pierrehumbert, R. T., 1991: Large-scale horizontal mixing in planetary atmospheres. *Phys. Fluids,* **3A,** 1250–1260.

——, 1994: Tracer microstructure in the large-eddy dominated regime. *Chaos Applied to Fluid Mixing,* H. Aref and M. S. El Naschie, Eds., Pergamon, 347–366.

——, 1998: Lateral mixing as a source of subtropical water vapor. *Geophys. Res. Lett.,* **25,** 151–154.

——, 2000: Lattice models of advection-diffusion. *Chaos,* **10** (6), 61–74.

——, and H. Yang, 1993: Global chaotic mixing on isentropic surface. *J. Atmos. Sci.,* **50,** 2462–2480.

Pope, S. B., and E. S. C. Ching, 1993: Stationary probability density functions: An exact result. *Phys. Fluids A,* **5** (7), 1529–1531.

Pumir, A., B. Shraiman, and E. D. Siggia, 1991: Exponential tails and random advection . *Phys. Rev. Lett.,* **66,** 2984–2987.

Putti, M., W. W.-G. Yeh, and W. Mulder, 1990: A triangular finite volume approach with high-resolution upwind terms for the solution of ground water transport equations. *Water Resour. Res.,* **26,** 2865–2880.

Rothstein, D., E. Henry, and J. P. Gollub, 1999: Persistent patterns in transient chaotic fluid mixing. *Nature,* **401,** 770–772.

Shraiman, B. I., and E. D. Siggia, 1994: Lagrangian path integrals and fluctuations in random flows. *Phys. Rev. E,* **49,** 2912–2927.

Sinai, Ya. G., and V. Yakhot, 1989: Limiting probability distributions of a passive scalar in a random velocity field. *Phys. Rev. Lett.,* **63,** 1962–1964.

Sreenivasan, K. R., and R. A. Antonia, 1997: The phenomenology of small-scale turbulence. *Ann. Rev. Fluid Mech.,* **29,** 435–472.

Tan, D. G. H., P. H. Haynes, A. R. MacKenzie, and J. A. Pyle, 1998: The effects of fluid-dynamical stirring and mixing on the deactivation of stratospheric chlorine. *J. Geophys. Res.,* **103** (D1), 1585–1605.

van Leer, B., 1977: Towards the ultimate conservative difference scheme, IV: A new approach to numerical convection. *J. Comput. Phys.,* **23,** 276–299.

Warhaft, Z., 2000: Passive scalars in turbulent flows. *Ann. Rev. Fluid Mech.,* **32,** 203–240.

Waugh, D. W., and R. A. Plumb, 1994: Contour advection with surgery: A technique for investigating fine scale structure in tracer transport. *J. Atmos. Sci.,* **51,** 530–540.

——, and Coauthors, 1994: Transport out of the lower stratospheric Arctic vortex by Rossby wave breaking. *J. Geophys. Res.,* **99,** 1071–1088.

Yakhot, V., S. A. Orszag, S. Balachandar, E. Jackson, Z. She, and L. Sirovich, 1990: Phenomenological theory of probability distributions in turbulence. *J. Sci. Comput.,* **5,** 199–221.